Meridional Overturning Circulations Driven by Surface Wind and Buoyancy Forcing

MICHAEL J. BELL

Met Office, Exeter, United Kingdom

(Manuscript received 15 December 2014, in final form 7 July 2015)

ABSTRACT

The meridional overturning circulation (MOC) can be considered to consist of a downwelling limb in the Northern Hemisphere (NH) and an upwelling limb in the Southern Hemisphere (SH) that are connected via western boundary currents. Steady-state analytical gyre-scale solutions of the planetary geostrophic equations are derived for a downwelling limb driven in the NH solely by surface heat loss. In these solutions the rates of the water mass transformations between layers driven by the surface heat loss determine the strength of the downwelling limb. Simple expressions are obtained for these transformation rates that depend on the most southerly latitudes where heat loss occurs and the depths of the isopycnals on the eastern boundary. Previously derived expressions for the water mass transformation rates in subpolar gyres driven by the Ekman upwelling characteristic of the SH are also summarized. Explicit expressions for the MOC transport and the depths of isopycnals on the eastern boundary are then derived by equating the water mass transformations in the upwelling and downwelling limbs. The MOC obtained for a ''single-basin'' two-layer model is shown to be generally consistent with that obtained by Gnanadesikan. The model's energetics are derived and discussed. In a world without a circumpolar channel in the SH, it is suggested that the upwelling limb would feed downwelling limbs in both hemispheres. In a world with two basins in the NH, if one of them has a strong halocline the model suggests that the MOC would be very weak in that basin.

1. Introduction

The meridional overturning circulation (MOC) in the Atlantic Ocean is part of a complex global circulation in which dense water formed by surface cooling in the North Atlantic flows in deep western boundary currents into the Southern Hemisphere (SH) before resurfacing south of the Antarctic Circumpolar Current (ACC) in a region of surface warming (Marshall and Speer 2012). Despite intensive study there are still differing conceptual views of the dynamics and energetics of this ''conveyor belt'' circulation (Huang 2010, his section 5.4). One point that is clear is that, as explained in Wunsch and Ferrari (2004) and Vallis (2006, his section 15.2), consideration of the energy budget shows that it is very unlikely that a consistent dynamical model of the MOC could be developed that is driven solely by surface buoyancy fluxes. Radko and Kamenkovich (2011), Drijfhout et al. (2013), and Schloesser et al. (2014) provide helpful reviews of the modern understanding of this circulation.

Following Cox (1989), various modeling studies have shown that the wind stresses in the South Atlantic have an important influence on the Atlantic MOC. Toggweiler and Samuels (1995) emphasized the role of the zonal-mean Ekman transport at the northern edge of the Drake Passage. Based on analyses of simplified ocean general circulation model simulations by Döös and Webb (1994), Toggweiler and Samuels (1995, 1998), Hasumi and Suginohara (1999), and Tsujino and Suginohara (1999), Webb and Suginohara (2001, p. 213) concluded that ''a large fraction of the water mass conversion, associated with the upwelling branch of the thermohaline circulation, occurs in the surface layers of the Southern Ocean.'' Klinger et al. (2003, 2004) provide further study of similar numerical experiments.

Building on ideas about the momentum balance in the circumpolar channel, as presented, for example, by Rintoul et al. (2001), Gnanadesikan (1999, hereinafter G99) proposed a simple model for the strength of the MOC in which the strength of the overturning transport in the Southern Ocean is determined by the northward Ekman

Corresponding author address: Dr. Mike Bell, Met Office, Fitzroy Rd., Exeter, EX1 3PB, United Kingdom.
E-mail: mike.bell@metoffice.gov.uk

DOI: 10.1175/JPO-D-14-0255.1

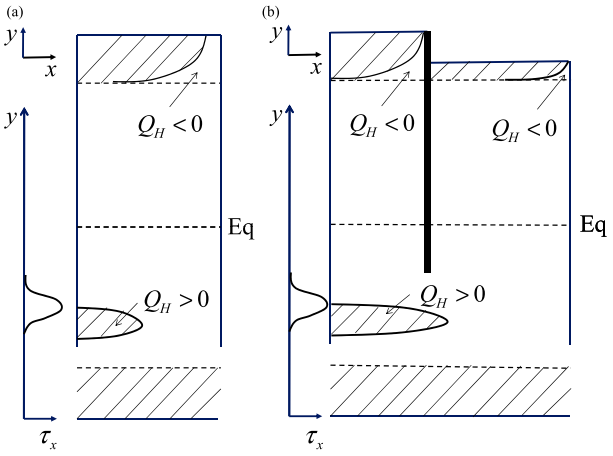

FIG. 1. (a) Depiction of the simplest ocean domain for which solutions are derived. The ocean occupies a rectangular basin spanning the equator with a periodic channel at its southern boundary. The model has only two isopycnal layers. The lower layer shoals or outcrops in the diagonally shaded regions. The surface heat flux into the ocean Q_H is only nonzero in the two regions shown. The zonal wind stress $\tau_x(y)$ is shown on the left of the figure. (b) The two-basin configuration discussed in section 8b. The basins are separated by a continent that extends to about 30°S.

transport in the channel and the net southward transport by the time-varying eddies at middepths. Gnanadesikan closed his model of the MOC transports by using scaling arguments relating the strength of the baroclinic western boundary current in the North Atlantic and the diabatic mixing at the base of the thermocline to the depth of the thermocline. In G99 the strength of the MOC is determined by a cubic equation for the depth of the thermocline at midlatitudes and is proportional to the square of this depth.

Samelson (2009), Radko and Kamenkovich (2011), and Nikurashin and Vallis (2011, 2012) have developed a number of numerical and analytical models of the MOC consistent with the ideas of G99. All these models represent the ocean by a single basin and a circumpolar channel in the SH as in Fig. 1a. They take the wind stress to be a maximum either within or at the northern edge of the channel so that the water mass transformations in the upwelling branch of the MOC that are driven by Ekman currents take place in the channel. The flow in the channel is taken to be zonally symmetric, and eddy transports make important contributions to the net (residual) flow. The depth of the isopycnals along the eastern boundary was found by Samelson (2009) to be nearly flat, and this boundary condition is used in Radko and Kamenkovich (2011) and implicit in Nikurashin and Vallis (2012). The water mass transformations resulting from high-latitude cooling are somewhat crudely represented in these models. Samelson (2009) represents it by relaxing the depth of his upper layer toward a value that is specified as a function of latitude. In Radko and Kamenkovich (2011), solutions are calculated first taking the MOC strength to be prespecified and later taking it to be proportional to the depth of the upper layer on the eastern boundary as in G99. Nikurashin and Vallis (2012) take the surface buoyancy field to be prescribed as a function of latitude and project it downward convectively in the basin to the level of neutral buoyancy.

Schloesser et al. (2012, 2014) have investigated the dynamics of the downwelling limb of the circulation in the North Atlantic using both a general circulation model and simplified analytical models. Their analysis starts with the phases of the spinup of the circulation from rest, which was also the starting point for this study (Bell 2011). The downwelling circulation is driven by meridionally varying surface temperatures, and the circulation is closed either by diapycnal upwelling or by flows at the southern boundary. Their analytical results are obtained for a two-layer model with the temperature of the upper layer set equal to the atmospheric surface temperature that entrains/detrains water into/from the lower layer in a manner that differs in detail from but is somewhat similar to that employed in this paper. Using a no normal flow eastern boundary condition, Schloesser et al. (2012) derive an expression for the overturning transport in the downwelling limb of the circulation that is somewhat similar to the expressions derived below in section 3 and the appendix.

The first aim of this paper is to derive simple expressions determining the rate of water mass transformations in the downwelling branch of the MOC from solutions to the planetary geostrophic equations (PGEs) using more physically based parameterizations of surface heat fluxes than those used by Samelson (2009), Radko and Kamenkovich (2011), and Nikurashin and Vallis (2012). The second aim is to combine these solutions with those for the upwelling limb of the MOC in the SH derived in Bell (2015b, hereinafter B15) and to compare and contrast the resulting expression for the strength of the MOC with that obtained by G99. The final aim of the paper is to outline how these calculations of the MOC can be extended to calculate the MOC for other configurations, particularly configurations with more than one ocean basin in the Northern Hemisphere (NH).

The simplest physical configuration for which solutions are obtained is illustrated in Fig. 1a. Following many previous authors (e.g., Greatbatch and Lu 2003), the ocean domain is represented as a single basin that is closed in the NH and has a periodic channel in the SH, and the ocean itself is represented by a small number of isopycnal layers (only two layers in Fig. 1a). Unlike many previous studies the strong surface westerlies in

the SH are specified to be a maximum well to the north of the channel, as they are in reanalyses (Radko and Marshall 2006), and the basin is taken to span almost 360° of longitude. To simplify the calculations, the surface wind stress is taken to be zonal and to be zero in the latitudes of the channel. The atmospheric surface temperature is taken to vary with latitude being colder at high latitudes than at the equator.

The nature of the solutions that are obtained when the surface temperature varies only with latitude is indicated by the shaded regions in Fig. 1a, which represent the regions in which the lower isopycnal layer either shoals or outcrops. The surface winds in the SH drive Ekman upwelling south of the wind stress maximum that causes the upper layer to shoal in the west of the basin. It is assumed that the surface atmosphere is warm enough at these latitudes for this to result in a surface heat flux into the ocean Q_H, which is positive and transforms water from the lower layer into water in the upper layer in this region of shoaling. Within the channel the flow is purely zonal and in thermal wind balance with the density field that outcrops to the south. The formulation of the buoyancy forcing used and the motivation for and derivation of these solutions for the SH have been presented in B15. These solutions with a subpolar gyre to the north of Drake Passage and an entirely separate zonal flow within the channel do not resemble the flow in the Southern Ocean very closely. But B15 suggests that if the wind stress field illustrated in Fig. 1a were moved southward, the westward flow in the southern half of the gyre would also move south and "merge" with the eastward flow in the channel to leave a single circumpolar flow that deflects sharply northward immediately to the east of Drake Passage. The solutions capture an east–west asymmetry in the net surface heat fluxes at about 50°S, which is prominent in a number of surface flux products (see Fig. 5.2 of Josey et al. 2013).

Along the eastern boundary of the ocean basin the boundary conditions used imply that the upper-layer depth does not change with latitude. As a result, at high latitudes in the NH where the surface atmosphere is sufficiently cold there is a region of substantial heat loss where water in the surface layer is transformed into water in the lower layer. Global steady-state solutions are obtained by choosing the depth of the upper layer on the eastern boundary so that the heat lost from the upper layer at the surface in the NH is equal to the heat gained in the SH. It is assumed that northern and western boundary currents close the interior circulations. One can imagine that nearer the equator than the regions discussed in this paper additional warmer water layers overlie the layers discussed here.

The rest of this paper is structured as follows: Section 2 briefly summarizes the formulation of the model; B15 gives a more detailed discussion. Section 3 presents simple analytical calculations of the water mass transformations that occur at high latitudes when the model is driven in the NH solely by surface cooling. The conceptual summary of the results for water mass transformations driven by Ekman upwelling in the SH derived in B15 is described in section 4. Section 5 presents a two-layer model of the MOC obtained by combining the above solutions for the NH and SH. Section 6 compares the model's formulation and results with those of G99, and section 7 discusses the model's energetics. Section 8 discusses MOCs in a world without a circumpolar channel in the SH and in a world with two basins, one of which has a strong halocline. Section 9 summarizes and discusses the simplifications used in the paper.

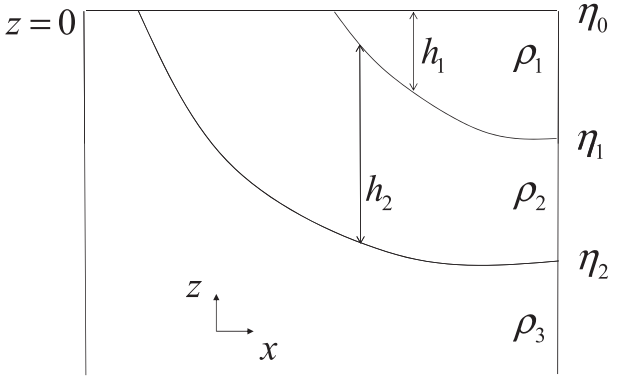

FIG. 2. Vertical section through a model with three layers. The variables x and z are coordinates that increase eastward and with height, respectively. The height $z = 0$ at the ocean surface, h_i is the depth of the ith layer, and η_i is the height of the interface at the base of the ith layer measured from $z = 0$.

An analysis of a similarly derived three-layer model of the MOC, which may be of interest to mathematically minded readers, is presented in Bell (2015a). The solutions and derivations for the three-layer model are conceptually and qualitatively similar to those for the two-layer model presented here. In particular the depths of the two interfaces between the three layers are determined by the condition that the net surface heat flux into each layer should be zero and the total MOC transport is of similar magnitude to that of the two-layer model.

2. Governing equations

The PGEs will be taken to govern the motions in the ocean interior (i.e., outside side-wall boundary layers). These equations are appropriate for large-scale motions in the ocean with a small Rossby number (see, e.g., Vallis 2006, his sections 3.3 and 5.2). For simplicity they are written in Cartesian coordinates with x increasing eastward and y increasing northward. Figure 2 illustrates

the notation that will be used for the case of an ocean with three layers. The variable h_i denotes the depth of the ith layer, and η_i is the height of the internal interface at the bottom of the ith layer measured from the constant geopotential surface $z = 0$. Variations in the depth of the ocean bathymetry $H(x, y)$ are assumed not to affect the motions; H may vary in regions where the lowest layer is at rest (reduced gravity) but is taken to be flat in regions where the lowest layer is directly forced (either by buoyancy or wind forcing). The density, geopotential, and horizontal velocities of the ith layer are denoted by ρ_i, ϕ_i, and $\mathbf{u}_i = (u_i, v_i)$, respectively. Using the rigid-lid approximation,

$$\eta_0 = 0, \tag{1}$$

and the layer depths and heights of the interfaces are related by

$$h_i = \eta_{i-1} - \eta_i, \quad 1 \le i \le N. \tag{2}$$

Defining the reduced gravities by

$$\rho_0 g_i = g(\rho_{i+1} - \rho_i), \quad 1 \le i < N, \tag{3}$$

where g is gravity, hydrostatic balance gives

$$\phi_{i+1} = \phi_i + g_i \eta_i, \quad 1 \le i < N. \tag{4}$$

The planetary geostrophic approximations to the horizontal momentum and continuity equations are then given by

$$f\mathbf{k} \times \mathbf{u}_i = -\nabla\phi_i + \frac{\boldsymbol{\tau}_i}{\rho_0 h_i}, \quad \text{and} \tag{5}$$

$$\frac{\partial h_i}{\partial t} + \nabla \cdot (h_i \mathbf{u}_i) = Q_{i,i+1} - Q_{i-1,i}. \tag{6}$$

In (5)–(6), which will be taken to apply for $1 \le i \le N$, $f = 2\Omega \sin\varphi$ is the Coriolis parameter, where Ω is the earth's rotation rate and φ is the latitude, $\mathbf{k}$ is the unit vector parallel to the z axis, and $\boldsymbol{\tau}_i = (\tau_{ix}, \tau_{iy})$ is the turbulent momentum flux absorbed in the ith layer (the wind stress on the layer if it is at the surface and sufficiently deep). In (6), $Q_{i,i+1}$ is the volume flux per unit area of water transformed from that of layer $i + 1$ into that of layer i as a result of the surface buoyancy fluxes across the ocean surface and mixing processes. Transfer of water into or out of additional layers at the top or bottom is not allowed, so

$$Q_{0,1} = Q_{N,N+1} = 0. \tag{7}$$

The formulation of the parameterization of $Q_{i,i+1}$ used here is discussed in detail in B15. The solutions derived in this paper have no freshwater fluxes, and for this case

$$Q_{i,i+1} = \frac{\alpha_T Q_i^H}{c_P(\rho_{i+1} - \rho_i)}, \tag{8}$$

where Q_i^H is the net heat flux, α_T is the thermal expansion coefficient, and c_p is the specific heat capacity of the water. When layer i is at the surface and the salinities in layers i and $i + 1$ are the same, for surface cooling Q_i^H will be parameterized by

$$Q_i^H = r_Q(T_A - T_i), \quad T_A < T_{i+1}, \tag{9}$$

in which $T_A(x, y)$ is an imposed atmospheric surface temperature, T_i is the temperature of the ith layer, and r_Q is the Haney coefficient. This formulation requires the surface cooling to form water that is denser than that in the layer below the surface before convection occurs. Section 8b discusses a case in which the salinities of the two layers differ, and (9) needs to be modified accordingly. Where the atmosphere surface temperature is warmer than that of the surface layer, the effective surface heating and diabatic mixing are taken to reduce with the surface layer depth divided by a mixing length λ_Q, and Q_i^H is specified by

$$Q_i^H = r_Q(T_A - T_i)\mathrm{e}^{\eta_i/\lambda_Q}, \quad T_A > T_i. \tag{10}$$

There is taken to be no heat flux for other surface temperatures:

$$Q_i^H = 0, \quad T_{i+1} < T_A < T_i. \tag{11}$$

A model with only a small number of layers that uses (11) is likely to have zero values of $Q_{i,i+1}$ over quite wide regions of the domain. So the fluxes that are obtained using the above parameterization in a two-layer model are of limited fidelity. This is one of the main motivations for the derivation of the N-layer surface cooling solution presented in the appendix. Together (9) and (11) result in a surface flux field that has discontinuities where the ith layer is at the surface along lines where $T_A = T_{i+1}$. For some purposes it certainly would be preferable to respecify (9) to avoid this, but the solutions discussed in this paper are robust to such discontinuities.

This paper will only consider steady-state solutions so the effects of time-mean eddy transports $\overline{h_i' u_i'}$ in (6) are not taken into account. A simple parameterization of small-scale vertical mixing similar to that used by Radko and Kamenkovich (2011) could be included in the model but has also been omitted. It will be assumed that the eastern boundary layers are unable to absorb any normal flow so that no normal flow boundary conditions apply to all the layers. It will also be assumed that the wind stress parallel

to the boundary is zero (as is the case when the winds are zonal and the boundaries lie due north–south). Denoting the eastern boundary by $x_E(y)$ and using (5) and (4), this implies that the geopotentials and the heights of the interfaces are constant along eastern boundaries:

$$\phi_i[x_E(y), y] = \phi_i^0 \equiv \phi_{iE}, \quad \text{and} \tag{12}$$

$$\eta_i[x_E(y), y] = \eta_i^0 \equiv \eta_{iE}. \tag{13}$$

Northern and western boundary layers will be assumed to be able to absorb and recirculate whatever flow is determined from the eastern boundary conditions and the interior equations (Huang and Flierl 1987).

The velocities $\mathbf{u}_i$ in (5) can be diagnosed from ϕ_i so (5) and (6) can be reduced to a single equation for each layer by multiplying (5) by h_i and substituting the resulting expression for $h_i\mathbf{u}_i$ into (6). Doing this and setting the time derivative in (6) to zero, one obtains

$$J\left(\phi_i, \frac{h_i}{f}\right) = Q_{i,i+1} - Q_{i-1,i} - C_i, \quad 1 \le i \le N, \tag{14}$$

where J denotes the Jacobian derivative, which for any ϕ and ψ is given by

$$J(\phi, \psi) \equiv \frac{\partial \phi}{\partial x}\frac{\partial \psi}{\partial y} - \frac{\partial \phi}{\partial y}\frac{\partial \psi}{\partial x}, \tag{15}$$

and C_i is an expression for the Ekman pumping in the ith layer given by

$$\rho_0 C_i \equiv \nabla \times \left(\frac{\boldsymbol{\tau}_i}{f}\right). \tag{16}$$

The total Ekman pumping C is calculated from the total wind stress $\boldsymbol{\tau}$, as in (16).

The area integral of the rate of transformation of water from layer j to layer i, which is a volume flux with units of cubic meters per second, will be denoted by

$$I_Q(i,j) \equiv \iint Q_{i,j}\, dx\, dy. \tag{17}$$

These integrals for the NH and the SH are of primary importance because they describe/determine the MOC (calculated in density space rather than depth space) across the equator.

3. Water mass transformations driven in the NH solely by surface cooling

A particularly simple and informative set of analytical steady-state solutions can be obtained when the surface wind forcing is small enough in comparison to the surface heat loss to be ignored. This approximation can be made for a narrow basin, like the Atlantic, when $|Q_{1,2}| \gg |C|$ and hence C is negligible on the rhs of (14). The restriction to narrow basins is necessary because the wind field modifies the path of the characteristics in wide basins (see, e.g., Schloesser et al. 2014; B15). In the North Atlantic, taking $\tau \approx 0.06\,\mathrm{N\,m^{-2}}$ and $\Delta y \approx 2 \times 10^6\,\mathrm{m}$, and using (16), one finds that $|C| \approx 3 \times 10^{-7}\,\mathrm{m^3\,s^{-1}}$. Using $T_1 = 10°\mathrm{C}$ and $T_2 = 4°\mathrm{C}$, one finds [e.g., using Gill (1982, his appendix 3)] that $\alpha_T \approx 1.3 \times 10^{-4}\,\mathrm{K^{-1}}$, $c_p \approx 4 \times 10^3\,\mathrm{J\,kg^{-1}\,K^{-1}}$, and $\rho_2 - \rho_1 \approx 0.83\,\mathrm{kg\,m^{-3}}$. Using these values in (8) gives $Q_{1,2} \approx 4 \times 10^{-8} Q_1^H$, where Q_1^H is expressed in watts per square meter. Since the net heat flux in the North Atlantic is of the order of $60\,\mathrm{W\,m^{-2}}$, neglect of the surface wind stresses is reasonably well founded. The terms T_A and Q_i^H will be allowed to vary with both longitude x and latitude y in this section.

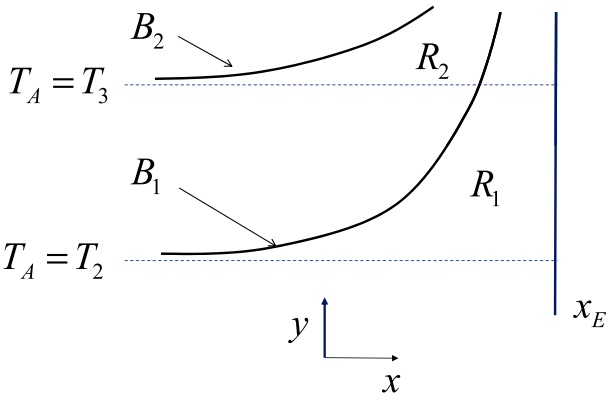

FIG. 3. Depiction of the regions R_i and boundaries B_i for the surface cooling calculation. Layer i outcrops along B_i. Region R_i is bounded to the west by B_i to the south by $T_A = T_{i+1}$ and to the east by $x = x_E$ when $i = 1$ and by B_{i-1} when $i > 1$.

a. *Solutions in the layer at the surface next to the eastern boundary*

Consider first the solution for region R_1 that is illustrated and defined in Fig. 3 and its caption. As only the two upper layers are directly forced, the lower layers can be taken to be at rest and hence

$$\phi_3 = \phi_{3E} = 0, \tag{18}$$

the constant value of ϕ_{3E} being taken to be zero for convenience. The steady-state solutions of (4) and (14) for the two active layers must then satisfy

$$\phi_2 = -g_2\eta_2, \tag{19a}$$

$$\phi_1 = -g_1\eta_1 - g_2\eta_2, \tag{19b}$$

$$J\left(\phi_1, \frac{-\eta_1}{f}\right) = Q_{1,2}, \quad \text{and} \tag{20}$$

$$J\left(\phi_2, \frac{\eta_1 - \eta_2}{f}\right) = -Q_{1,2}. \tag{21}$$

Summing (20) and (21), using (19), and recalling that $J(\psi, \psi) = 0$ for any ψ, one finds that

$$\frac{\beta}{f^2}\frac{\partial}{\partial x}(g_1\eta_1^2 + g_2\eta_2^2) = 0. \tag{22}$$

Integrating (22) w.r.t. x from the eastern boundary gives the Sverdrup relation

$$g_1\eta_1^2 + g_2\eta_2^2 = g_1\eta_{1E}^2 + g_2\eta_{2E}^2. \tag{23}$$

Using the definition of the Jacobian and (23), one then sees that

$$\begin{aligned} 2g_2\eta_2 J(\eta_2, \eta_1) &= g_2 J(\eta_2^2, \eta_1) \\ &= -g_1 J(\eta_1^2, \eta_1) = 0. \end{aligned} \tag{24}$$

Multiplying (20) by η_2, using (19b) to eliminate ϕ_1, and then using (22) and (24), one obtains

$$\beta g_1\eta_1(\eta_2 - \eta_1)\frac{\partial \eta_1}{\partial x} = -f^2\eta_2 Q_{1,2}. \tag{25}$$

As is well known (e.g., Pedlosky 2012), (23) and (25) together define a first-order ordinary differential equation for η_1 that can be solved using elementary methods. This holds even though $Q_{1,2}$ is still an unspecified function of the coordinates x and y.

A remarkably simple expression [see (32) below] for the area integral of $Q_{1,2}$ in region R_1 can be obtained by first integrating (25) w.r.t. x after writing (23) in the form

$$g_2^2\eta_2^2 = g_1 g_2(a_E^2 - \eta_1^2), \quad \text{and} \tag{26}$$

$$g_1 a_E^2 \equiv g_1\eta_{1E}^2 + g_2\eta_{2E}^2. \tag{27}$$

Assuming that the surface heat flux is strong enough to make the upper layer outcrop before it reaches the western boundary and using (26) in (25), one obtains

$$\int_{R_1} f^2 Q_{1,2}\, dx = -\beta\int_0^{\eta_{1E}}\left(g_1\eta_1 + \frac{\sqrt{g_1 g_2}\,\eta_1^2}{\sqrt{a_E^2 - \eta_1^2}}\right) d\eta_1. \tag{28}$$

Choosing to define a_E to be negative allows one to define positive angles ϑ and ϑ_E such that

$$a_E \sin\vartheta \equiv \eta_1, \quad a_E \sin\vartheta_E \equiv \eta_{1E}, \tag{29}$$

and to calculate the second integral on the rhs of (28):

$$\int_{R_1} Q_{1,2}\, dx = -\frac{\beta K_{1,2}}{2f^2}, \quad \text{and} \tag{30}$$

$$K_{1,2} \equiv g_1\eta_{1E}^2 - \sqrt{g_1 g_2}\, a_E^2\left(\vartheta_E - \frac{1}{2}\sin 2\vartheta_E\right). \tag{31}$$

TABLE 1. Evaluations of $\csc\varphi - 1$.

φ (°N)	$\csc\varphi - 1$
90	0
85	0.0038
80	0.0154
75	0.035
70	0.064
65	0.103
60	0.155
55	0.221
50	0.305

The quantity $K_{1,2}$ only depends on the layer depths along the eastern boundary and so is independent of latitude. Consequently, (30) can be integrated with respect to latitude:

$$I_Q(1,2) = \int_{R_1} Q_{1,2}\, dx\, dy = \frac{K_{1,2}}{4\Omega} L(\varphi_2; \varphi_P), \quad \text{and} \tag{32}$$

$$L(\varphi_2; \varphi_P) = -4\Omega\int_{y_2}^{y_P}\frac{\beta}{2f^2}dy = -\int_{\varphi_2}^{\varphi_P}\frac{\cos\varphi}{R\sin^2\varphi}R\, d\varphi. \tag{33}$$

In (33), φ_2 is a latitude fractionally poleward of that at which $T_A = T_2$, and φ_P is the most poleward latitude of the eastern boundary. To be more precise, φ_2 is the first latitude at which water in layer 1 is transformed into water in layer 2 sufficiently rapidly for layer 1 to outcrop within the basin. The transition between there being no heat flux and very strong heat fluxes in this model is very sharp because of the formulation of the parameterization of heat loss in (9), so in this paper the latitude of outcropping will be taken to be the most southerly latitude at which $T_A(x, y) = T_2$.

Expression (32) for the key quantity $I_Q(1,2)$ should be viewed as a dynamical result. The horizontal divergences in the upper and lower layers resulting from the exchange of water between them must be balanced by changes in the planetary vorticity of water in the two layers as given by (20) and (21). This determines the east–west slope in the depths of the isopycnals [see (25)] and hence the latitudinal dependence of the zonal integral [(30)] of the volume flux $Q_{1,2}$.

The integral in (33) is easily calculated:

$$L(\varphi_2; \varphi_P) = [\csc\varphi]_{\varphi_2}^{\varphi_P} \approx -(\csc\varphi_2 - 1). \tag{34}$$

Table 1 provides evaluations of $\csc\varphi - 1$ as a function of latitude from which L can be calculated. It is clear that the approximation in (34) is accurate to within 10% for evaluations of L with $\varphi = 60$°N in basins where the eastern boundary extends poleward of 80°N. For simplicity of presentation, this approximation will be made hereafter, and L will be written as $L(\varphi_2)$.

b. Solutions in the lower layers of a three-layer model

Consider now the solution for a three-layer model in region R_2 in Fig. 3. At the eastern edge of this region, that is, at the boundary B_1 between regions R_1 and R_2, $\eta_{1B_1} = 0$ and, from (18), $\phi_3 = 0$. Using these points with (23) gives

$$g_2\eta_{2B_1}^2 = g_1\eta_{1E}^2 + g_2\eta_{2E}^2, \quad \phi_{3B_1} = 0. \tag{35}$$

Within region R_2 itself the steady-state solutions of (4) and (14) for the two remaining layers must satisfy

$$\phi_2 = \phi_3 - g_2\eta_2, \tag{36}$$

$$J\left(\phi_2, \frac{-\eta_2}{f}\right) = Q_{2,3}, \quad \text{and} \tag{37}$$

$$J\left(\phi_3, \frac{H+\eta_2}{f}\right) = -Q_{2,3}. \tag{38}$$

Summing (37) and (38), assuming that the bathymetry is flat, and integrating w.r.t. x westward from B_1 [i.e., repeating the steps in the derivation of (23)], one obtains the Sverdrup relation for region R_2 in the form:

$$g_2\eta_2^2 + 2H\phi_3 = g_2\eta_{2B_1}^2 + 2H\phi_{3B_1}. \tag{39}$$

Combining (39) and (35) then gives

$$g_2\eta_2^2 + 2H\phi_3 = g_1\eta_{1E}^2 + g_2\eta_{2E}^2. \tag{40}$$

Equation (40) implies that $J(\eta_2, \phi_3) = 0$ and by similar steps to those in the derivation of (25), one finds that

$$\beta g_2\eta_2(H+\eta_2)\frac{\partial\eta_2}{\partial x} = -f^2HQ_{2,3}. \tag{41}$$

Integrating w.r.t. x and then w.r.t. y as in the derivation of (32) and assuming that the surface heat fluxes in region R_2 poleward of latitude φ_3 are strong enough to make layer 2 outcrop, one then finds that

$$I_Q(2,3) = \frac{M_{2,3}}{4\Omega}L(\varphi_3), \quad \text{and} \tag{42}$$

$$M_{2,3} \equiv g_2\eta_{2B_1}^2\left(1 + \frac{2\eta_{2B_1}}{3H}\right). \tag{43}$$

Table 2 presents evaluations of the latitude-independent factors in (32) that contribute to $I_Q(1, 2)$ and those in (42) that contribute to $I_Q(2, 3)$ for a three-layer model whose layer temperatures are 10°, 4°, and −2°C and whose salinity is 35 ppt in all layers.

To combine Tables 1 and 2 it is necessary to specify the lowest latitudes at which the transformations from 10° to 4°C water and from 4° to −2°C water take place. The surface air temperature in the North Atlantic is colder on the western side of the basin, so the latitudes should be based on the air temperatures there. The surface air temperature east of the Grand Banks (at 50°N) varies from 0°C in February to 10°C in July, so the steady-state calculation that has been posed is clearly an oversimplification. Given this position, a reasonable approach is to specify some plausible values for these latitudes and to interpret the results with caution. It will be assumed in this and later calculations that 4°C water will start to form at 60°N and −2°C water at 70°N, noting that a more southerly latitude of 50°N could plausibly be used for the formation of 4°C water and that this would double the amount of water transformed.

TABLE 2. Evaluations of terms in (32) and (42) using (31) and (43) for selected values of η_{1E} and η_{2E}. Other values used are $g_1 = 2g_2 = 0.008\,\text{m s}^{-2}$, $H = 4000\,\text{m}$.

$-\eta_{1E}$ (m)	$-\eta_{2E}$ (m)	$K_{1,2}/(4\Omega)$ (Sv)	$M_{2,3}/(4\Omega)$ (Sv)
500	1000	4.96	17.1
1000	2000	19.8	50.7
1500	3000	44.6	74.8

With the above choices taking the depths of the layer interfaces to be 1000 and 2000 m, one sees from Tables 1 and 2 that the diapycnal mass transport from layers 1 to 2, $I_Q(1, 2)$, would be $0.154 \times 19.8\,\text{Sv} = 3.0$ Sverdrups (Sv; $1\,\text{Sv} \equiv 10^6\,\text{m}^3\,\text{s}^{-1}$), while that from layers 2 to 3 would be $0.064 \times 50.7\,\text{Sv} = 3.2\,\text{Sv}$. Clearly the transports in this model depend strongly on the depths of the interfaces on the eastern boundary and the most equatorward latitude at which surface cooling starts to generate water for each of the layers.

The zonal scale of the solutions of (25) and (41) depends on the volume fluxes between the layers Q and varies with latitude in proportion to βf^{-2}. At high latitudes this scale becomes very small, and the surface cooling is likely to become concentrated near the eastern boundary and to give rise to a baroclinic eastern boundary current. This current might be interpreted in the Atlantic as the Norwegian Coastal Current (LaCasce 2004). The typical shapes of the isopycnal gradients in these currents are illustrated in Bell (2011).

Using proof by induction one can derive similar solutions to those above for models with more layers. These solutions are not used subsequently in this paper and so are simply stated in the appendix; the proof follows the steps already described.

4. Solutions for Ekman-driven upwelling

B15 presents numerical solutions obtained using the three-layer PGEs for subpolar gyre circulations in wide basins driven by strong Ekman upwelling centered at

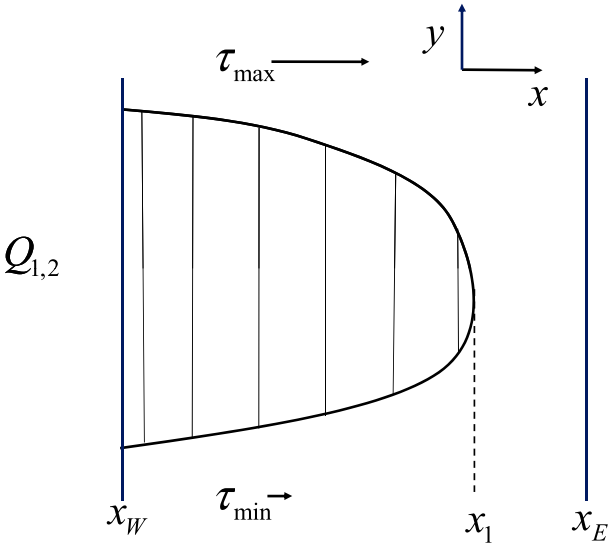

FIG. 4. The conceptual picture used to summarize the numerical results for a two-layer model. It shows the outcropping region obtained in the subpolar gyre inside which the net surface heat flux is controlled by the wind stress curl C.

55°S. The conceptual summary of the results for a two-layer model is presented in Fig. 4. A subpolar gyre is obtained between the latitude to the north where the zonal wind stress is a maximum and that to the south where it is a minimum. The range in the wind stress will be denoted by $\tau_{\text{range}} \equiv \tau_{\max} - \tau_{\min}$. The upper layer shoals along the curve shown, which lies within the latitudes of maximum and minimum wind stress. The eastern edge of this curve lies at x_1, which is given by

$$2f^2C(x_1 - x_E) = -\beta g_1 \eta_{1E}^2. \tag{44}$$

Within the region where the upper layer shoals, if the water in the surface layer is colder than the atmosphere (i.e., $T_1 < T_A$), the rate of transformation of water from layer 2 to layer 1, that is, $Q_{1,2}$, is found to be controlled by the Ekman pumping C defined in (16), with $Q_{1,2} \approx C$. An approximate expression for the area integral of the rate at which layer 1 obtains water (a flux with units of cubic meters per second) is then given by

$$I_O = \iint_{\text{SH}} Q_{1,2}\, dx\, dy \approx C(x_1 - x_W)\Delta y, \tag{45}$$

where Δy is the north–south extent of the outcropping region and SH denotes the Southern Hemisphere.

Away from the equator to a good approximation $f\rho_0 C = -\partial\tau_x/\partial y$, so one can write

$$f\rho_0 C\Delta y = -\gamma\tau_{\text{range}} \tag{46}$$

and expect $\frac{1}{2} \le \gamma \le 1$. Calculating γ by substituting (46) into (45) and using values of I_O from the numerical solutions confirms that it is appropriate to use this range of values of γ and that $\gamma = 0.9$ is a good choice for solutions in which the shoaling occurs in midbasin. Combining (44)–(46) gives

$$\begin{aligned} I_O &\approx C(x_1 - x_E + x_E - x_W)\Delta y \\ &= -\frac{\beta g_1 \eta_{1E}^2}{2f^2}\Delta y - \frac{\gamma\tau_{\text{range}}(x_E - x_W)}{f\rho_0}. \end{aligned} \tag{47}$$

Note that the first term on the rhs of (47) is negative, while the second term is positive and equal to γ times the integral across the basin of the difference between the northward Ekman transports $[\tau/(\rho_0 f)]$ at which the wind stress is a maximum and a minimum.

5. A two-layer model of the MOC

Following Walin (1982), De Szoeke (1995), and G99, consider the implications of requiring the volume transferred from the upper to the lower layer accompanying surface cooling in the NH to equal the volume transferred from the lower to the upper layer accompanying the warming of cold upwelling water in the SH [I_O as given by (47)]. Adapting (42) and (43) to the two-layer model, the rate at which volume is lost from layer 1 to 2 in the NH is given by

$$I_L \equiv -\iint_{R_1} Q_{1,2}\, dx\, dy = -\frac{M_{1,2}}{4\Omega} L(\varphi_2), \quad \text{and} \tag{48}$$

$$M_{1,2} = g_1 H^2 \left(\frac{\eta_{1E}}{H}\right)^2 \left(1 + \frac{2\eta_{1E}}{3H}\right) \approx g_1 \eta_{1E}^2. \tag{49}$$

The final approximation above assumes that $h_{1E} \ll H$. This assumption is made here for simplicity. A similar calculation that does not make this approximation is presented in Bell (2015a).

Equating I_L as given by (48) with I_O as given by (47) one obtains

$$\left(\frac{\eta_{1E}}{H}\right)^2 \left[L(\varphi_2)\sin\varphi_S - \frac{\Delta y \cot\varphi_S}{R}\right] = 2\frac{\gamma\tau_{\text{range}}(x_E - x_W)}{\rho_0 g_1 H^2}, \tag{50}$$

in which φ_S is a latitude representative of that at which water upwells in the SH, and the two bracketed terms on the lhs are each nondimensional.

Figure 5a illustrates how the height of the interface, η_{1E} inferred from (50), depends on the strength of the wind forcing τ_{range} and the latitude φ_2 at which lower-layer water starts to form; when $g_1 = 0.008\ \text{m s}^{-2}$ (as is the case when the water in the two layers has the same salinity and temperatures of 10° and 4°C), the upwelling region

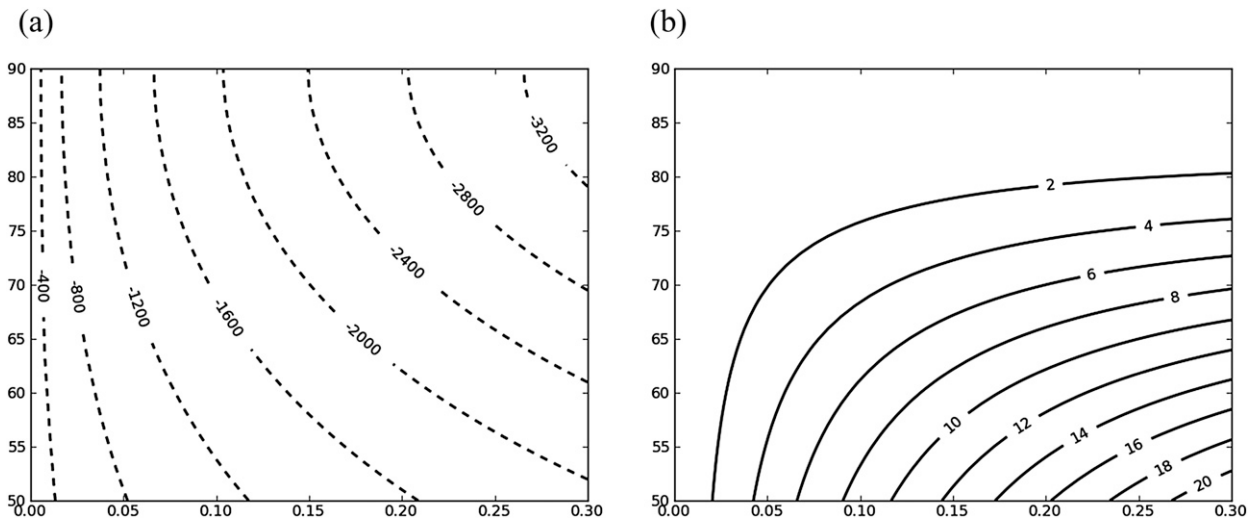

FIG. 5. (a) The height (m) of the interface on the eastern boundary η_{1E}, calculated using (50) and (b) the strength of the MOC (Sv) I_L, calculated using (48) and the full expression for $M_{1,2}$ in (49), as a function of the range of wind stresses (N m^{-2}) in the SH τ_{range} (on the abscissa) and the latitude φ_2 (°N) at which lower-layer water first forms in the NH, with other parameter values as described in the text.

is centered at 55°S, so $\varphi_S = -55°$, and the width of this upwelling region is 10°, so that $\Delta y \approx R/6$, $\gamma = 0.9$, and $x_E - x_W = 2 \times 10^7$ m. Figure 5b illustrates how the strength of the MOC (Sv), I_L calculated using (48) and the full expression for $M_{1,2}$ in (49), varies using the same parameters as in Fig. 5a. The values in this figure should be compared with measurements of the MOC transport at about 60°N rather than the transport obtained from the RAPID array at 26.5°N that is bolstered by the heat losses in the Gulf Stream at about 40°N. Figure 5a shows that when the wind stress is weak or water mass transformation in the NH is confined to high latitudes, η_{1E} depends mainly on the range of the wind stress in the SH. The strength of the MOC increases both as the wind stress in the SH increases and as the latitude where cold water can form in the NH moves southward. When $\varphi_2 =$ 60°N and $\tau_{\text{range}} = 0.15\,\text{N}\,\text{m}^{-2}$, $I_L \approx 8.9$ Sv.

6. Comparisons with G99

G99 infers the strength of the overturning circulation in the NH, T_n in his notation, from a calculation of the western boundary current involving the depth of the thermocline D, which assumes that there is a north–south gradient in the depth of the thermocline in the NH. The expression (48) for the corresponding quantity I_L in this paper has been derived without making this assumption but has terms g_1, η_{1E}, and Ω that correspond to g', D, and $\beta \approx 2\Omega/R$ in G99's expression for T_n. This agreement is very welcome because the transport in the western boundary current needs to match the water mass transformations by the surface fluxes for the circulations to be self-consistent. [Appendix A of Fürst and Levermann (2012) discusses a number of alternative scalings for T_n.] The main difference between the expressions for T_n and I_L is that G99's expression for T_n does not have a term corresponding to $L(\varphi_2)$ in I_L. There also appears to be a quantitative difference between the formulas, with G99's choice for his constant of proportionality C giving T_n a factor of 4 larger than would be calculated using the formulas for I_L and the standard choices of parameters in this paper, but two factors may account for this discrepancy. First, G99 chooses C by fitting to the MOC from a general circulation model. This MOC would include a wider range of water masses than the 4° to 10°C range considered here. Second, as already noted, the choice of φ_2 used here may be conservative. Choosing a value of 50°N in place of 60°N would double the strength of the circulation.

G99's argument for the overturning circulation in the SH, T_s in his notation, depends on there being a Southern Ocean channel, whereas the expression (47) was derived for a basin. The formulas for T_s and I_O nevertheless have a similar dependence on a zonally integrated Ekman flux. In the case of G99, this is a circumpolar Ekman flux within the Drake Passage, whereas in this paper it is the difference between the basinwide Ekman fluxes at the latitudes where the wind stress is a maximum and a minimum. The correction to the Ekman flux depends on the eddy bolus transport in G99, proportional to $A_I D$, A_I being the Gent–McWilliams diffusion parameter, while in this paper the correction depends on the distance between the eastern edge of the shoaling region and the eastern

boundary and is proportional to η_{1E}^2. Gnanadesikan et al. (2003) note that a quadratic dependence on D for the correction can produce a better fit to the SH transports in their coarse-resolution ocean model than a linear dependence. G99 also includes a parameterization of diapycnal upwelling through the low-latitude pycnocline. As mentioned earlier, this could easily have been included in (6) or it could be directly included in (50) but has been omitted.

In summary, despite the differences in their derivation and interpretation, the models of the MOC given here and in G99 produce results that are generally consistent. Clearly the expression for the transport in the SH derived by G99 (T_s) could be equated with that for the NH derived in this paper (I_L) to obtain an additional simple model of the MOC.

7. Energetics of the *N*-layer model

As the energetics of the MOC have had a significant influence on ideas about how it is driven (Vallis 2006; Wunsch and Ferrari 2004; Hughes et al. 2009; Tailleux 2009) and the energetics of the model described in this paper are very straightforward, it is pertinent to describe them. The derivations here stem from sections 5.7 and 6.7 of Gill (1982).

The kinetic energy equation is obtained by taking the scalar product of the horizontal momentum equation [(5)] with $\rho_0 h_i \mathbf{u}_i$:

$$0 = -\rho_0 h_i \left(u_i \frac{\partial \phi_i}{\partial x} + v_i \frac{\partial \phi_i}{\partial y} \right) + (u_i \tau_{xi} + v_i \tau_{yi}). \quad (51)$$

The equation for the evolution of potential energy is obtained by multiplying (6) by $\rho_0 \phi_i$:

$$\rho_0 \phi_i \frac{\partial h_i}{\partial t} + \rho_0 \phi_i \nabla \cdot (h_i \mathbf{u}_i) = \rho_0 \phi_i (Q_{i,i+1} - Q_{i-1,i}). \quad (52)$$

As the upper and lower interfaces are stationary, using (2) and (4) the first term on the lhs of (52) when summed over all layers reduces to the familiar form for the rate of change of potential energy:

$$\begin{aligned} &\rho_0 \sum_{i=1}^{N} \phi_i \frac{\partial}{\partial t}(-\eta_i + \eta_{i-1}) \\ &= \rho_0 \sum_{i=1}^{N} -\phi_i \frac{\partial \eta_i}{\partial t} + (\phi_{i-1} + g_{i-1}\eta_{i-1}) \frac{\partial \eta_{i-1}}{\partial t} \\ &= \rho_0 \sum_{i=1}^{N-1} g_i \frac{\partial}{\partial t} \frac{\eta_i^2}{2}. \end{aligned} \quad (53)$$

When (51) and (52) are added together, the first term on the rhs of (51) and the second term on the lhs of (52) can clearly be combined into the divergence of the horizontal flux $\rho_0 \phi_i h_i \mathbf{u}_i$. The final term on the rhs of (51) is then the energy input by the surface wind stress, and the term on the rhs of (52) is the potential energy input by the surface buoyancy fluxes. If at a particular point (x, y) the two layers directly affected by the buoyancy flux are layers p and $p + 1$, then the total input to the potential energy by the buoyancy flux $Q_{p,p+1}$, summed over the two layers affected, is given by $\rho_0(\phi_p - \phi_{p+1})Q_{p,p+1}$. From (4) this is equal to $-\rho_0 g_p \eta_p Q_{p,p+1}$. Hence, when the surface heating occurs in shallow layers at the surface and the cooling occurs in deep surface layers (as envisaged in this paper), the buoyancy forcing is a net sink of potential energy.

Two further points should be made before leaving the energetics. First, the expressions described above only apply to the ocean interior, not to the boundary current regions where one would expect there to be some additional dissipation of energy. Second, the energetics only place one constraint on the motions. When this constraint is sufficient to arrest any flow, it is of great interest, but in situations where it is not, its importance diminishes.

8. More complex configurations

a. *MOCs with and without an Antarctic Circumpolar Channel*

Since Cox (1989), most discussions of the impact of the Southern Ocean on the MOC have studied the combined impact of an open circumpolar channel and strong westerly winds. This subsection discusses the MOCs that would be obtained when the winds are present in the absence of a circumpolar channel (i.e., if the Drake Passage were closed). This is of interest both because paleo evidence shows that the continents have moved considerably and suggest that the channel has been closed in the past (Hill et al. 2013) and because it suggests a slightly different interpretation of the role of the channel in the present-day MOC. The eastern boundary of the Pacific in that case would run from high northern latitudes to high southern latitudes as it does in the "Ridge" experiments performed by Enderton and Marshall (2009). One would then expect the convective mixing discussed in section 3 to take place in the SH as well as the NH. This means that the Ekman upwelling in the SH would need to return this volume flux from both hemispheres. If one assumes that the convective flux would be the same in the two hemispheres, one would calculate the resulting circulations in the two-layer model by setting the upwelling flux I_O, as given by (45), equal to twice I_L, as given by (48). The interface depths on the eastern boundary would then be shallower

than in the solution with $I_O = I_L$, so the total volume transfer to the upper layer in the upwelling region would increase but the return volume flux in the NH would decrease. This calculation highlights the role of the circumpolar channel in disconnecting the waters in high southern latitudes from the MOC and the role of the eastern boundary condition in generating the MOCs through maintaining isopycnal depths that are independent of latitude and hence introducing warm waters to high latitudes where they must be converted to cold water by surface heat loss.

b. *Discussion of a simple two-basin World Ocean*

Johnson et al. (2007) have extended the G99 model to include a representation of net evaporation at low latitudes and precipitation at high latitudes, and it is natural to ask whether the present analysis could provide any insight into why the cross-equatorial MOC is so much stronger in the Atlantic than the Pacific Ocean.

The sea surface salinity in the North Pacific is about 2 psu less than that in the North Atlantic (Huang 2010, his Fig. 11.5), and the North Pacific has a strong halocline, which is not present in the North Atlantic, with surface salinities more than 1 psu lower than in the water below. Of course it is possible that these differences are a consequence rather than the cause of the reduced MOC in the Pacific, but the paragraphs below argue that these salinity differences would reduce the magnitude of convective mixing and hence weaken the MOC in the Pacific, as envisaged in the experiment described in section 6 of Greatbatch and Lu (2003).

For simplicity the following argument considers only the salinity differences arising in the halocline. More specifically suppose that the depths of the isopycnals at the eastern boundaries in the Pacific and the Atlantic are the same and that the salinities in the upper layer in the North Pacific are ΔS psu lower than those in the Atlantic, while the salinities of all lower layers are the same as those in the Atlantic surface layer.

The parameterization of the convective overturning in (9) needs to be adjusted so that overturning does not occur until the water in the surface layer at the atmospheric surface temperature is denser than the water in the layer below. The reduction in surface temperature ΔT°C required to compensate for the increase in density due to a salinity increase of ΔS psu across the halocline is given by

$$\rho\alpha_T \Delta T = \alpha_S \Delta S. \tag{54}$$

Using a thermal expansion coefficient $\rho\alpha_T = 0.135\,\mathrm{kg\,m^{-3}\,K^{-1}}$ appropriate for cooling water from 10° to 4°C and $\alpha_S = 0.8\,\mathrm{kg\,m^{-3}\,psu^{-1}}$ gives $\Delta T = 6\Delta S\,^{\circ}\mathrm{C\,psu^{-1}}$.

The atmospheric surface temperature at which the upper layer would become convectively unstable in the North Pacific would then be $6\Delta S$ °C lower than that in the North Atlantic. This implies that the latitude at which convective mixing of the surface layer with the layer below would commence would be much farther north in the Pacific than the Atlantic. Table 1 shows that the total water mass transformed between layers by convective mixing depends very strongly on the latitude at which it commences; the transformation is reduced by a factor of 10 if the latitude is changed from 60° to 80°N. So the observed salinity difference could weaken the MOC in the Pacific substantively.

Two additional factors could reduce the water mass transformations in the real-world Pacific. First, it does not extend much beyond 60°N. Second, it is wide compared with the Atlantic, so the upward displacement of the isopycnals by the winds in the subpolar gyre is likely to be greater in the Pacific than the Atlantic. At latitudes where the convective mixing is on the western side of the basin, this would reduce the amount of water in the upper layer that could be transformed into lower-layer waters.

The above arguments assume that the depths of the isopycnals on the eastern boundaries of the Pacific and Atlantic are the same. In general this will not be the case, but the following argument shows that it is true to a good approximation for the simple case of a two-layer ocean in the world illustrated in Fig. 1b, which has two continents, one (America) being specified as before and one (Africa/Asia) extending only to 30°S (which is the latitude of the southern tip of Africa). The argument exploits the facts that the zonal-mean zonal wind is approximately zero at 30°S and that the velocity along the coast in the western boundary current is to a very good approximation in geostrophic balance. Integrating the zonal component of (5) for the upper layer across the entire Pacific basin at 30°S, the above points imply that the total northward transport (including that in the western boundary layer) by the upper layer in the Pacific at 30°S is given by

$$\int_W^E h_1 v_1\,dx = \int_W^E \frac{-\eta_1}{f}\frac{\partial}{\partial x}(-g_1\eta_1 + \phi_2)\,dx$$
$$= \frac{g_1}{2f}(\eta_{1E}^2 - \eta_{1W}^2) - \int_W^E \frac{\eta_1}{f}\frac{\partial \phi_2}{\partial x}\,dx. \tag{55}$$

This northward transport is equal to the rate of volume lost from the upper layer in the Pacific due to heat loss I_L, as given by (48) and (49). Taking $|L(\varphi_2)| \le 0.15$ in (48), noting that $f = -\Omega$ at 30°S and using (55), one obtains

$$-\frac{g_1}{\Omega}(\eta_{1E}^2 - \eta_{1W}^2) - \int_W^E \frac{\eta_1}{f}\frac{\partial \phi_2}{\partial x}\,dx = I_L \le 0.15\frac{g_1\eta_{1E}^2}{4\Omega}. \tag{56}$$

If the final term on the lhs of the equals sign of (56) is negligible, (56) implies that η_{1W}^2 is within 10% of η_{1E}^2. The magnitude of this final term can be shown to be of order $(h_1/H)I_L$ and hence negligible by considering the northward transport across 30°S in the lower layer into the Pacific. This must satisfy

$$-I_L = \int_W^E h_2 v_2 \, dx = \int_W^E \frac{(\eta_1 - \eta_2)}{f} \frac{\partial \phi_2}{\partial x} dx \approx \frac{H}{f} \Delta\phi_2 , \qquad (57)$$

where $\Delta\phi_2$ is representative of east–west differences in ϕ_2. Using this scaling for ϕ_2 in (56) confirms that the last term on the lhs of the equals sign in (56) is of order $(h_1/H)I_L$.

It is then reasonable to take the value of h_{1W} in the Pacific at 30°S to be equal to h_{1E} in the Atlantic. The above argument then implies that the depths of the isopycnals in this simple two-layer model for a two-basin world would agree to within 10%.

9. Summary

The main aim of this paper is to use relatively simple solutions for gyre-scale circulations in the NH and SH that are driven by surface wind stresses and/or Haney-type heat fluxes [specified by (9)–(11)] to derive quantitative estimates of the strength of the main MOC in world oceans such as those illustrated in Fig. 1. This parameterization of the heat fluxes has a reasonable physical basis and is significantly different from that used in the studies mentioned in the introduction (B15, his section 2b).

Section 3 and the appendix derive analytical solutions for 2-, 3- and N-layer models of the downwelling branch of the North Atlantic that are driven in the NH solely by heat loss to the atmosphere. Simple expressions for the area-integrated volume transfer between layers, defined by (17), are obtained for two active layers [(32), in which the terms are given by (31) and (34)], the lowest layer of a three-layer model [(42) and (43)], and the nth layer of a reduced gravity model with more than $n + 1$ layers [(A5) and (A6)]. All these formulas involve the product of a term that depends only on the depths of the layer interfaces on the eastern boundary and a second term that depends primarily on the latitudes at which the atmospheric surface temperature T_A first becomes equal to the temperatures of the subsurface layers. These formulas are valid for any specification of T_A as a function of latitude and longitude and determine the strength of the downwelling branch of the MOC.

Section 4 summarizes the conceptual picture (Fig. 4) for subpolar gyres driven by the Ekman upwelling of the SH winds that was derived from numerical integrations in a previous paper (B15). The winds drive cold water to the surface on the western side of the basin and largely control the heat extracted from the atmosphere there. Simple quantitative estimates of the rate of transformation of water in terms of northward Ekman transports integrated across the basin and the depths of the isopycnals on the eastern boundary for a two-layer model are given by (47).

Section 5 derives a simple two-layer model of the MOC by requiring the water lost from the upper layer in the North Atlantic to be equal to the water transformed back into the upper layer in the Ekman upwelling region of the SH. This determines a linear relationship [(50)] between the range of the Ekman transports in the SH and the square of the interface depth on the eastern boundary. The latter is approximately proportional to the strength of the MOC. Section 6 compares this model of the MOC with that of G99 and shows that they are generally consistent. From Fig. 5 one can see that the model predicts that an increase in the maximum wind stress in the SH would, in the absence of other changes, deepen the thermocline and strengthen the MOC in the steady-state solution. Similarly if atmospheric surface temperatures in the NH warm but those in the SH are relatively unchanged, the model suggests that the steady-state MOC would weaken.

Section 7 recalls the relatively transparent energetics of a layered model and makes it clear that the circulation draws its energy from the surface wind forcing. Section 8 briefly discusses a World Ocean in which an eastern boundary extends from pole to pole and suggests that convective mixing would occur at high latitudes in both hemispheres. Consideration of that case gives a different perspective on the roles of the Southern Ocean channel and the eastern boundary conditions in shaping the MOC. Section 8 also discusses a two-basin ocean in which one of the basins has a strong halocline like that in the Pacific. It is shown that according to the model presented here a halocline of the observed strength would greatly reduce the MOC in the basin containing it. If near-surface salinities are reduced at all northerly latitudes, one would expect the most southerly latitude of dense water formation to move northward, and the model suggests that the steady-state MOC would weaken.

Most of the assumptions and simplifications made in this paper were discussed in the final section of B15. Four simplifications are, however, worth highlighting, the first being that only steady-state solutions have been considered. More specifically, seasonal variations have not been taken into account despite the fact that the atmospheric forcing of the Northern Hemisphere branch of the overturning will vary greatly with the

season and the total overturning cannot be estimated properly using annual average surface atmospheric temperatures. An analysis similar in concept to that of Johnson and Marshall (2002) is required to estimate the annual-mean water mass transformation rate. The second simplification is the neglect of wind forcing and interactions with sloping bathymetry in the downwelling branch of the circulation. Although neglect of the winds was partially justified through a scaling argument, it was motivated at least in part by the desire to obtain quantitative estimates whose scaling properties could be readily understood. The third simplification is that the northern and western boundary layers in this paper are assumed to be entirely passive. Huang and Flierl (1987), Salmon (1998), and Pedlosky and Spall (2005) provide valuable discussions of these boundary layers and some of their subtleties. The fourth simplification is the restriction of the wind stresses to the north of the channel in the SH. Clearly a better representation of the ACC and its interaction with the wind-driven Ekman upwelling circulation than that discussed here is highly desirable.

Acknowledgments. This work was supported by the Joint U.K. DECC/Defra Met Office Hadley Centre Climate Programme (GA01101). The author is particularly grateful to David Marshall, Geoff Vallis, and Andy White for their advice and to two anonymous reviewers and the editor whose comments helped to improve the presentation of the paper considerably.

APPENDIX

Solutions in Models with More Layers

This appendix records the solution obtained for a model with more than $n + 1$ layers in the region R_n defined in Fig. 3 where the wind stresses are negligible and the ocean is losing heat to the atmosphere. The solution satisfies

$$g_n\eta_n^2 + g_{n+1}\eta_{n+1}^2 = W(n+1), \quad \text{and} \tag{A1}$$

$$\beta g_n \eta_n(\eta_{n+1} - \eta_n)\frac{\partial \eta_n}{\partial x} = -f^2\eta_{n+1}Q_{n,n+1}, \tag{A2}$$

where

$$W(n) \equiv \sum_{i=1}^{n} g_i\eta_{iE}^2 \tag{A3}$$

and on the eastern boundary of region n (i.e., on B_{n-1})

$$g_n\eta_n^2|_{B_{n-1}} = W(n), \quad \eta_{n+1}|_{B_{n-1}} = \eta_{n+1E}. \tag{A4}$$

Repeating the steps in the derivation of (32) one finds that

$$I_Q(n,n+1) = \int_{R_n} Q_{n,n+1}\,dx\,dy = \frac{K_{n,n+1}}{4\Omega}L(\varphi_{n+1}), \tag{A5}$$

$$K_{n,n+1} \equiv W(n) - \sqrt{\frac{g_{n+1}}{g_n}}\left(\vartheta_n - \frac{1}{2}\sin 2\vartheta_n\right)W(n+1), \quad \text{and} \tag{A6}$$

$$\sin^2\vartheta_n \equiv \frac{W(n)}{W(n+1)}. \tag{A7}$$

The above derivation has again assumed (see section 3) that the surface heat flux is strong enough that poleward of the most southerly latitude at which $T_A = T_{n+1}$, the nth layer will outcrop. It also requires that the nth layer does not become deeper than the $n + 1$th layer at any point in the domain. This can readily be checked using (A4), which with (A3) gives a simple expression for the maximum depth reached by the base of the nth layer. For example, denoting the ratio of g_1 and g_2 by μ_g (i.e., $\mu_g \equiv g_1/g_2$) and the ratio of η_{1E} and η_{2E} by μ_h (i.e., $\mu_h \equiv \eta_{1E}/\eta_{2E}$), the maximum depth reached by the base of the second layer is $\sqrt{(1+\mu_g\mu_h^2)}$ times its depth at the eastern boundary. With $\mu_g = 2$ and $\mu_h = ½$, this gives a maximum depth of about $-1.22\eta_{2E}$.

REFERENCES

Bell, M. J., 2011: Ocean circulations driven by meridional density gradients. *Geophys. Astrophys. Fluid Dyn.*, **105**, 182–212, doi:10.1080/03091929.2010.534468.

——, 2015a: Meridional overturning circulations driven by surface wind and buoyancy forcing. Met Office Hadley Centre Tech. Note 98, 19 pp.

——, 2015b: Water mass transformations driven by Ekman upwelling and surface warming in subpolar gyres. *J. Phys. Oceanogr.*, **45**, 2356–2380, doi:10.1175/JPO-D-14-0251.1.

Cox, M. D., 1989: An idealized model of the World Ocean. Part I: The global scale water masses. *J. Phys. Oceanogr.*, **19**, 1730–1752, doi:10.1175/1520-0485(1989)019<1730:AIMOTW>2.0.CO;2.

De Szoeke, R. A., 1995: A model of wind- and buoyancy-driven ocean circulation. *J. Phys. Oceanogr.*, **25**, 918–941, doi:10.1175/1520-0485(1995)025<0918:AMOWAB>2.0.CO;2.

Döös, K., and D. J. Webb, 1994: The Deacon cell and the other meridional cells in the Southern Ocean. *J. Phys. Oceanogr.*, **24**, 429–442, doi:10.1175/1520-0485(1994)024<0429:TDCATO>2.0.CO;2.

Drijfhout, S. S., D. P. Marshall, and H. A. Dijkstra, 2013: Conceptual models of the wind-driven and thermohaline circulation. *Ocean Circulation and Climate: A 21st Century Perspective*, G. Siedler et al., Eds., Academic Press, 257–282.

Enderton, D., and J. Marshall, 2009: Explorations of the atmosphere–ocean–ice climates on an aquaplanet and their meridional energy transports. *J. Atmos. Sci.*, **66**, 1593–1611, doi:10.1175/2008JAS2680.1.

Fürst, J. J., and A. Levermann, 2012: A minimal model for wind- and mixing-driven overturning: Threshold behavior for both driving mechanisms. *Climate Dyn.*, **38**, 239–260, doi:10.1007/s00382-011-1003-7.

Gill, A. E., 1982: *Atmosphere–Ocean Dynamics.* Academic Press, 662 pp.

Gnanadesikan, A., 1999: A simple predictive model of the structure of the oceanic pycnocline. *Science*, **283**, 2077–2081, doi:10.1126/science.283.5410.2077.

——, R. D. Slater, and B. L. Samuels, 2003: Sensitivity of water mass transformation and heat transports to subgridscale resolution in coarse-resolution ocean models. *Geophys. Res. Lett.*, **30**, 1967, doi:10.1029/2003GL018036.

Greatbatch, R. J., and J. Lu, 2003: Reconciling the Stommel box model with the Stommel–Arons model: A possible role for Southern Hemisphere wind forcing? *J. Phys. Oceanogr.*, **33**, 1618–1632, doi:10.1175/2411.1.

Hasumi, H., and N. Suginohara, 1999: Atlantic deep circulation controlled by heating in the Southern Ocean. *Geophys. Res. Lett.*, **26**, 1873–1876, doi:10.1029/1999GL900420.

Hill, D. J., A. M. Haywood, P. J. Valdes, J. E. Francis, and D. J. Lunt, 2013: Paleogreographic controls on the onset of the Antarctic Circumpolar Current. *Geophys. Res. Lett.*, **40**, 5199–5204, doi:10.1002/grl.50941.

Huang, R. X., 2010: *Ocean Circulation: Wind-Driven and Thermohaline Processes.* Cambridge University Press, 791 pp.

——, and G. R. Flierl, 1987: Two-layer models for the thermocline and current structure in subtropical/subpolar gyres. *J. Phys. Oceanogr.*, **17**, 872–884, doi:10.1175/1520-0485(1987)017<0872:TLMFTT>2.0.CO;2.

Hughes, G. O., A. McHogg, and R. W. Griffiths, 2009: Available potential energy and irreversible mixing in the meridional overturning circulation. *J. Phys. Oceanogr.*, **39**, 3130–3146, doi:10.1175/2009JPO4162.1.

Johnson, H. L., and D. P. Marshall, 2002: A theory for the surface Atlantic response to thermohaline variability. *J. Phys. Oceanogr.*, **32**, 1121–1132, doi:10.1175/1520-0485(2002)032<1121:ATFTSA>2.0.CO;2.

——, ——, and D. A. J. Sproson, 2007: Reconciling theories of a mechanically driven meridional overturning circulation with thermohaline forcing and multiple equilibria. *Climate Dyn.*, **29**, 821–836, doi:10.1007/s00382-007-0262-9.

Josey, S. A., S. Gulev, and L. Yu, 2013: Exchanges through the ocean surface. *Ocean Circulation and Climate: A 21st Century Perspective*, G. Siedler et al., Eds., Academic Press, 115–140.

Klinger, B. A., S. Drijfhout, J. Marotzke, and J. R. Scott, 2003: Sensitivity of basinwide meridional overturning to diapycnal diffusion and remote wind forcing in an idealized Atlantic–Southern Ocean geometry. *J. Phys. Oceanogr.*, **33**, 249–266, doi:10.1175/1520-0485(2003)033<0249:SOBMOT>2.0.CO;2.

——, ——, ——, and ——, 2004: Remote wind-driven overturning in the absence of the Drake Passage effect. *J. Phys. Oceanogr.,* **34**, 1036–1049, doi:10.1175/1520-0485(2004)034<1036:RWOITA>2.0.CO;2.

LaCasce, J. H., 2004: Diffusivity and viscosity dependence in the linear thermocline. *J. Mar. Res.*, **62**, 743–769, doi:10.1357/0022240042880864.

Marshall, J., and K. Speer, 2012: Closure of the meridional overturning circulation through Southern Ocean upwelling. *Nat. Geosci.*, **5**, 171–180, doi:10.1038/ngeo1391.

Nikurashin, M., and G. Vallis, 2011: A theory of deep stratification and overturning circulation in the ocean. *J. Phys. Oceanogr.*, **41**, 485–502, doi:10.1175/2010JPO4529.1.

——, and ——, 2012: A theory of the interhemispheric meridional overturning circulation and associated stratification. *J. Phys. Oceanogr.*, **42**, 1652–1667, doi:10.1175/JPO-D-11-0189.1.

Pedlosky, J., 2012: Theory of oceanic buoyancy driven flows. *Buoyancy-Driven Flows*, E. P. Chassignet, C. Cenedese, and J. Verron, Eds., Cambridge University Press, 52–117.

——, and M. A. Spall, 2005: Boundary intensification of vertical velocity in a β-plane basin. *J. Phys. Oceanogr.*, **35**, 2487–2500, doi:10.1175/JPO2832.1.

Radko, T., and J. Marshall, 2006: The Antarctic Circumpolar Current in three dimensions. *J. Phys. Oceanogr.*, **36**, 651–669, doi:10.1175/JPO2893.1.

——, and I. Kamenkovich, 2011: Semi-adiabatic model of the deep stratification and meridional overturning. *J. Phys. Oceanogr.*, **41**, 757–780, doi:10.1175/2010JPO4538.1.

Rintoul, S. R., C. Hughes, and D. Olbers, 2001: The Antarctic Circumpolar Current system. *Ocean Circulation and Climate*, 1st ed., G. Siedler, J. Church, and J. Gould, Eds., Academic Press, 271–302.

Salmon, R., 1998: *Lectures on Geophysical Fluid Dynamics.* Oxford University Press, 378 pp.

Samelson, R. M., 2009: A simple dynamical model of the warm-water branch of the middepth meridional overturning cell. *J. Phys. Oceanogr.*, **39**, 1216–1230, doi:10.1175/2008JPO4081.1.

Schloesser, F., R. Furue, J. P. McCreary, and A. Timmermann, 2012: Dynamics of the Atlantic meridional overturning circulation. Part 1: Buoyancy-forced response. *Prog. Oceanogr.*, **101**, 33–62, doi:10.1016/j.pocean.2012.01.002.

——, ——, ——, and ——, 2014: Dynamics of the Atlantic meridional overturning circulation. Part 2: Forcing by winds and buoyancy. *Prog. Oceanogr.*, **120**, 154–176, doi:10.1016/j.pocean.2013.08.007.

Tailleux, R., 2009: On the energetics of stratified turbulent mixing, irreversible thermodynamics, Boussinesq models, and the ocean heat engine controversy. *J. Fluid Mech.*, **638**, 339–382, doi:10.1017/S002211200999111X.

Toggweiler, J. R., and B. Samuels, 1995: Effect of Drake Passage on the global thermohaline circulation. *Deep-Sea Res.*, **42**, 477–500, doi:10.1016/0967-0637(95)00012-U.

——, and ——, 1998: On the ocean's large-scale circulation near the limit of no vertical mixing. *J. Phys. Oceanogr.*, **28**, 1832–1852, doi:10.1175/1520-0485(1998)028<1832:OTOSLS>2.0.CO;2.

Tsujino, H., and N. Suginohara, 1999: Thermohaline circulation enhance by wind forcing. *J. Phys. Oceanogr.*, **29**, 1506–1516, doi:10.1175/1520-0485(1999)029<1506:TCEBWF>2.0.CO;2.

Vallis, G. K., 2006: *Atmospheric and Oceanic Fluid Dynamics.* Cambridge University Press, 745 pp.

Walin, G., 1982: On the relation between sea-surface heat flow and thermal circulation in the ocean. *Tellus*, **34A**, 187–195, doi:10.1111/j.2153-3490.1982.tb01806.x.

Webb, D. J., and N. Suginohara, 2001: The interior circulation of the ocean. *Ocean Circulation and Climate*, 1st ed., G. Siedler, J. Church, and J. Gould, Eds., Academic Press, 205–214.

Wunsch, C., and R. Ferrari, 2004: Vertical mixing, energy and the general circulation of the oceans. *Annu. Rev. Fluid Mech.*, **36**, 281–314, doi:10.1146/annurev.fluid.36.050802.122121.